

# Particle Videos Revisited: Tracking Through Occlusions Using Point Trajectories

Adam W. Harley, Zhaoyuan Fang, and Katerina Fragkiadaki

Carnegie Mellon University

{aharley, zhaoyuaf, katef}@cs.cmu.edu



Figure 1. **Particle Videos.** Our method takes an RGB video as input, and estimates trajectories for any number of target pixels. Top-left: target pixels are marked with dots; bottom-left: estimated trajectories. Right: estimated trajectories overlaid on the first frame of the input.

## Abstract

*Tracking pixels in videos is typically studied as an optical flow estimation problem, where every pixel is described with a displacement vector that locates it in the next frame. Even though wider temporal context is freely available, prior efforts to take this into account have yielded only small gains over 2-frame methods. In this paper, we revisit Sand and Teller’s “particle video” approach, and study pixel tracking as a long-range motion estimation problem, where every pixel is described with a trajectory that locates it in multiple future frames. We re-build this classic approach using components that drive the current state-of-the-art in flow and object tracking, such as dense cost maps, iterative optimization, and learned appearance updates. We train our models using long-range amodal point trajectories mined from existing optical flow datasets that we synthetically augment with occlusions. We test our approach in trajectory estimation benchmarks and in keypoint label propagation tasks, and compare favorably against state-of-the-art optical flow and feature tracking methods.<sup>1</sup>*

## 1. Introduction

In 2006, Sand and Teller [21] wrote that there are two dominant approaches to motion estimation in video: feature matching and optical flow. This is still true today. In their paper, they proposed a new motion representation called a “particle video”, which they presented as a middle-ground between feature tracking and optical flow. The main idea is to represent a video with a set of particles that move across multiple frames, and leverage long-range temporal priors while tracking the particles.

Methods for feature tracking and optical flow estimation have greatly advanced since that time, but there has been relatively little work on estimating long-range trajectories at the pixel level. Feature correspondence methods [3, 32] currently work by matching the features of each new frame to the features of one or more source frames [14], without taking into account temporal context. Optical flow methods today produce such exceedingly-accurate estimates within pairs of frames [26] that the motion vectors can often be chained across time without much accumulation of error, but as soon as the target is occluded, it is no longer represented in the flow field, and tracking fails.

Particle videos have the potential to capture two key ele-

<sup>1</sup>Project page: <http://cs.cmu.edu/~aharley/particles>

ments missing from feature-matching and optical flow: (1) persistence through occlusions, and (2) multi-frame temporal context. If we attend to a pixel that corresponds to a point on the world surface, we should expect that point to exist across time, even if appearance and position and visibility all vary somewhat unpredictably. Temporal context is of course widely known to be relevant for flow-based methods, but prior efforts to take multi-frame context into account have yielded only small gains. Flow-based methods mainly use consecutive pairs of frames, and occasionally leverage time with a simple constant-velocity prior, which weakly conditions the current flow estimate on previous frames’ flow [19, 26].

We propose Deep Particle Video (DPV), a new particle video method, which takes a  $T$ -frame RGB video as input, along with the  $(x, y)$  coordinate of a target to track, and produces a  $T \times 2$  matrix as output, representing the positions of the target across the given frames. The model can be queried for any number of particles, at any positions within the first frame’s pixel grid. A defining feature of our approach, which differentiates it from both the original particle video method and modern flow methods, is that it makes an extreme trade-off between spatial awareness and temporal awareness. *Our model estimates the trajectory of every target independently.* Computation is shared between particles within a video, which makes inference fast, but each particle produces its own trajectory, without inspecting the trajectories of its neighbors. This extreme choice allows us to devote the majority of parameters into a module that simultaneously learns (1) temporal priors, and (2) an inference mechanism that *searches* for the target pixel’s location in all input frames. The value of the temporal prior is that it allows the model to *fail* its correspondence task at multiple intermediate frames. As long as the pixel is “found” at some sparse timesteps within the considered temporal span, the model can use its prior to estimate plausible positions for the remaining timesteps. This is helpful because appearance-based correspondence is impossible in some frames, due to occlusions, moving out-of-bounds, or difficult lighting.

We train our model entirely in synthetic data, which we call FlyingThings++, based on the FlyingThings [16] optical flow dataset. Our dataset includes multi-frame amodal trajectories of various lengths, with challenging synthetic occlusions caused by moving and static objects. In our experiments on both synthetic and real video data, we demonstrate that our particle trajectories are more robust to occlusions than flow trajectories—they can pick up an entity upon re-appearance—and also provide smoother and finer-grained correspondences than current feature-matching methods, thanks to its temporal prior. We also propose a method to link the model’s moderate-length trajectories into arbitrarily-long trajectories, relying on a

simultaneously-estimated visibility cue. Figure 1 displays sample outputs of our model on RGB videos from the DAVIS benchmark [18]. We plan to publicly release our code, model weights, and data.

## 2. Related Work

### 2.1. Optical flow

While earlier optical flow methods use optimization techniques to estimate motion fields between two consecutive frames [2, 24], recent methods learn such displacement fields supervised from synthetic datasets [5, 9]. Many recent works use iterative refinements for flow estimation by leveraging coarse-to-fine pyramids [23]. Instead of coarse-to-fine refinements, RAFT [26] mimics an iterative optimization algorithm, and estimates flow through iterative updates of a high resolution flow field based on 4D correlation volumes constructed for all pairs of pixels from per-pixel features. Inspired by RAFT, we also perform iterative updates of the position estimations using correlations as an input, but unlike RAFT we additionally update features.

Ren *et al.* [19] propose a fusion approach for multi-frame optical flow estimation. The optical flow estimates of previous frames are used to obtain multiple candidate flow estimations for the current timestep, which are then fused into a final prediction by a learnable module. In contrast, DPV explicitly reasons about multiframe context, and iteratively updates its estimates across all frames considered. Note that without using multiple frames, it is impossible to recover an entity after occlusion. Janai *et al.* [11] is closer to our method, since it uses 3 frames as multiframe context, and explicitly reasons about occlusions. That work uses a constant velocity prior [20] to estimate motion during occlusion. In contrast, DPV devotes a large part of the model capacity to learning an accurate temporal prior, and iteratively updates its estimates across all frames considered, in search of the object’s re-emergence from occlusion. Note that without using multiple frames, it is impossible to recover an entity after occlusion. Additionally, our model is the only work that aims to recover *amodal* trajectories that do not terminate at occlusions but rather can recover and re-connect with a visual entity upon its re-appearance.

### 2.2. Feature matching

Wang and Jabri *et al.* [10, 32] leverage cycle consistency of time for feature matching. This allows unsupervised learning of features by optimizing a cycle consistency loss on the feature space across multiple time steps in unlabelled videos. Lai *et al.* [14, 15] and Yang *et al.* [36] learn feature correspondence through optimizing a proxy reconstruction objective, where the goal is to reconstruct a target frame (color or flow) by linearly combining pixels from one or more reference frames. The combination weights are ob-

tained by computing affinities between the features from the target frame and features from the reference frame(s).

Instead of using proxy tasks, supervised approaches [7, 12, 31, 33] directly train models using ground truth correspondences across images. Features are usually extracted per-image and a transformer-based processor locates correspondences between images. In this work, we reason about point correspondences over a long temporal horizon, incorporating motion context, instead of using pairs of frames like these works.

## 3. Deep Particle Video (DPV)

### 3.1. Setup and overview

We name our model Deep Particle Video (DPV), taking conceptual inspiration from Particle Video [21]. DPV takes as input an RGB video with  $T$  frames, and the  $(x_1, y_1)$  coordinate of a single point on the first frame, indicating the target to track. As output, the model produces a  $T \times 3$  matrix, containing  $T$  tracked coordinates  $(x_t, y_t)$  across time, along with visibility/occlusion estimates  $v_t \in [0, 1]$ . The model can be queried for  $N$  target points in parallel, and some computation will be shared between them, but the model does not share information between the targets’ trajectories.

At training time, we query the model with points for which we have ground-truth trajectories and visibility labels. We supervise the model’s  $(x_t, y_t)$  outputs with a regression objective, and supervise  $v_t$  with a classification objective. At test time, the model can be queried for the trajectories of any number of points.

We use the words “point” and “particle” interchangeably to mean the things we are tracking, and use the word “pixel” more broadly to indicate any discrete cell on the image grid. Note that although the tracking targets are specified with single pixel coordinates, tracking successfully requires (at least) taking into account the local spatial context around the specified pixel, and therefore the model is somewhat sensitive to scale and resolution.

Our overall approach has four stages, somewhat similar to the RAFT optical flow method [26]: extracting visual features (Section 3.2), initializing a list of positions and features for each target (Section 3.3), locally measuring appearance similarity (Section 3.4), and repeatedly updating the positions and features for each target (Section 3.5). Figure 2 shows an overview of the method.

### 3.2. Extracting features

We begin by extracting features from every frame of the input video. In this step, each frame is processed independently with a 2D convolutional network (i.e., no temporal convolutions). The network produces features at 1/8 resolution.

### 3.3. Initializing each target

After computing feature maps for the video frames, we compute a feature vector for the target, by bilinearly sampling inside the first feature map at the first (given) coordinate, obtaining a feature vector  $f_1$ .

We use this sampled feature to initialize a trajectory of features, by simply tiling the feature across time, yielding a matrix  $\mathcal{F}^0$  sized  $T \times C$ , where  $C$  is the channel dimension. This initialization implies an appearance constancy prior.

We initialize the target’s trajectory of positions in a similar way. We simply copy the initial position across time, yielding a matrix  $\mathcal{X}^0$ , shaped  $T \times 2$ . This initialization implies a zero-velocity prior, which essentially assumes nothing about the target’s motion.

During inference, we will update the trajectory of features, tracking appearance changes, and update the trajectory of positions, tracking motion.

### 3.4. Measuring local appearance similarity

We would like to measure how well our trajectory of positions, and associated trajectory of features, matches with the pre-computed feature maps. We compute visual similarity maps by correlating each feature  $f^t$  with the feature map of the corresponding timestep, and then obtain “local” scores by bilinearly sampling a crop centered at the corresponding position  $(x_t, y_t)$ . This step returns patches of un-normalized similarity scores, where large positive values indicate high similarity between the target’s feature and the convolutional features at this location. We denote the initial set of scores as  $\mathcal{C}^0$ , shaped  $T \times P \cdot P$ , where  $P$  is the size of the patch extracted from each correlation map.

Similar to RAFT [26], we find it is beneficial to create a spatial pyramid of these score patches, to obtain similarity measurements at multiple scales. This makes our score matrix  $T \times P \cdot P \cdot L$ , where  $L$  is the number of levels in the pyramid.

### 3.5. Iterative updates

The main inference step for our model involves updating the sequence of positions, and updating the sequence of features. To perform this update, we take into account all of the information we have computed thus far: the position matrix  $\mathcal{X}^k$ , the feature matrix  $\mathcal{F}^k$ , and the correlation matrix  $\mathcal{C}^k$ , indicated here with superscript  $k$  to emphasize that these inputs will change across iterative inference steps.

Instead of using absolute positions  $\mathcal{X}^k$ , we subtract the given position  $(x_1, y_1)$  from each element of this matrix, making it into a matrix of displacements. (On the first iteration, it will in fact be all zeros, since  $\mathcal{X}^0$  is initialized from  $(x_1, y_1)$ .) Using displacements instead of absolute positions makes all input trajectories appear to start at  $(0, 0)$ , which makes our model translation-invariant. We additionally concatenate sinusoidal position encodings of the dis-

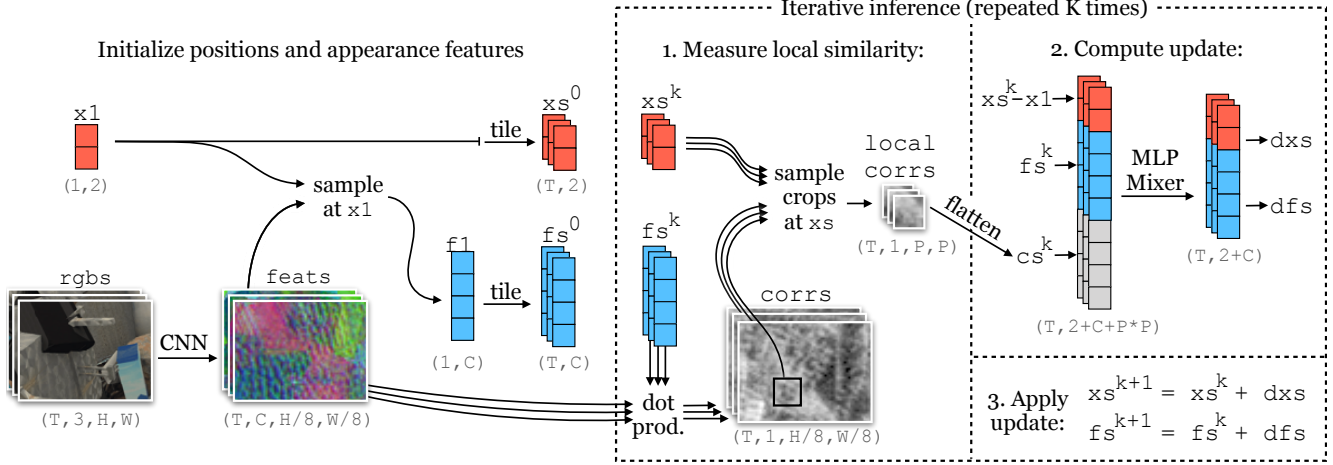


Figure 2. **Architecture of Deep Particle Video (DPV).** Given an RGB video as input, along with a location in the first frame indicating what to track, our model initializes a multi-frame trajectory, then computes features and correlation maps, and iteratively updates the trajectory and its corresponding sequence of features, with a deep MLP-Mixer model.

placements [30], motivated by the success of these encodings in vision transformers [4].

To process this broad set of inputs, we concatenate them all on the channel dimension, yielding a new matrix shaped  $T \times D$ , and process this with a 12-block MLP-Mixer [28], which is a parameter-efficient all-MLP architecture with design similarities to a transformer. As output, this module produces updates for the sequence of positions and sequence of features,  $d\mathcal{X}$  and  $d\mathcal{F}$ , which we apply with:

$$\begin{aligned} \mathcal{F}^{k+1} &= \mathcal{F}^k + d\mathcal{F}, \\ \mathcal{X}^{k+1} &= \mathcal{X}^k + d\mathcal{X}. \end{aligned} \quad (1)$$

After each update, we compute new correlation pyramids at the updated coordinates, using the updated features.

The update module is iterated  $K$  times. After the last update, the positions  $\mathcal{X}^K$  are treated as the final trajectory, and the features  $\mathcal{F}^K$  are sent to a linear layer to estimate per-timestep visibility logits  $\mathcal{V}$ .

### 3.6. Supervision

We supervise the model using the  $L_1$  distance between the ground-truth trajectory and the estimated trajectory (across iterative updates), with exponentially increasing weights, similar to RAFT [26]:

$$\mathcal{L}_{\text{main}} = \sum_k^K \gamma^{K-k} \|\mathcal{X}^k - \mathcal{X}^*\|_1, \quad (2)$$

where  $K$  is the number of iterative updates, and we set  $\gamma = 0.8$ . Note that this loss is applied even when the target is occluded, or out-of-bounds, which is possible since we are using synthetically-generated ground truth. This is the main

loss of the model, and the model can technically train using only this, although it will not learn visibility estimation and convergence will be slow.

On the model’s visibility estimates, we apply a cross entropy loss:

$$\mathcal{L}_{\text{ce}} = \mathcal{V}^* \log \mathcal{V} + (1 - \mathcal{V}^*) \log(1 - \mathcal{V}). \quad (3)$$

We find it accelerates convergence to directly supervise the score maps to peak in the correct location (i.e., the location of the true correspondence) when the target is visible:

$$\mathcal{L}_{\text{score}} = -\log(\exp(c_i) / \sum_j \exp(c_j)) \mathbb{1}\{\mathcal{V}^* \neq 0\}, \quad (4)$$

where  $c_j$  represents the match score at pixel  $j$ , and  $i$  is pixel index with the true correspondence.

We average all losses across all targets within a batch. We set the coefficient of every loss to 1.

### 3.7. Test-time trajectory linking

At test time, it is often desirable to generate correspondences over longer timespans than the training sequence length  $T$ . To generate these longer trajectories, we may repeat inference starting from any timestep along the estimated trajectory, treating  $(x_t, y_t)$  as the new  $(x_1, y_1)$ , and thereby “continuing” the trajectory up to  $(x_{t+T}, y_{t+T})$ . However, doing this naively (e.g., always continuing from the last timestep), can quickly cause tracking to drift.

It is first of all crucial to avoid continuing the trajectory from a timestep where the target is occluded. Otherwise, the model will switch to tracking the occluder. To avoid these identity switches, we make use of our visibility estimates, and seek the farthest timestep whose visibility

score is above a threshold. Note that seeking farthest visible timestep allows the model to skip past frames where the target was momentarily occluded, as long as the temporal span of the occlusion is less than the temporal span of the model ( $T$ ). Visibility estimates always begin near 1, since the model is trained assuming the provided  $(x_1, y_1)$  indicates the true target, so we exclude the first several timesteps from this selection process, forcing the model to choose a timestep from the later part of the trajectory. We initialize the threshold conservatively at 0.99, and decrease it in increments of 0.01 until a valid selection is found.

Even with visibility-aware trajectory linking, the model can “forget” what it was originally tracking, since the target initialization strategy involves bilinearly sampling at the new  $(x_1, y_1)$  location whenever a new link is added to the chain. We therefore employ a second strategy, which is simply to always initialize  $\mathcal{F}^0$  using the features found at the very first timestep. Intuitively, this locks the model into tracking the “original” target. This does create a slight mismatch between the target features and the convolutional feature maps on the current frame, but we find that this is effectively compensated for by the internal update mechanism. We have also tried a strategy of initializing with the last  $\mathcal{F}^K$  output by the model, but this leads to unstable behavior.

## 4. Implementation details

**CNN:** Our CNN uses the “BasicEncoder” architecture from the official RAFT codebase [27]. This architecture has a  $7 \times 7$  convolution with stride 2, then 6 residual blocks with kernel size  $3 \times 3$ , then a final convolution with kernel size  $1 \times 1$ . The CNN has an output dimension of  $C = 256$ .

**Local correlation pyramids:** We use three levels in our correlation pyramids, with radius 4. This translates to three  $9 \times 9$  correlation patches per timestep.

**MLP-Mixer:** The input to the MLP-Mixer is a sequence of relative coordinates, features, and correlation pyramids. The coordinates are made “relative” by subtracting the first position, meaning the first element of this sequence is  $(0, 0)$ , and other elements of the sequence can be interpreted as flow vectors originating from the first timestep’s absolute position. The per-timestep inputs are flattened, then treated as a sequence of vectors (i.e., “tokens”) for the MLP-Mixer. We use the MLP-Mixer architecture exactly as described in the original paper; at the end of the model there is a mean over the sequence dimension, followed by a linear layer that maps to a channel size of  $T \cdot (C + 2)$ .

**Updates:** We reshape the MLP-Mixer’s outputs into a sequence of feature updates and a sequence of coordinate updates. We apply the coordinate updates directly (with addition). We use separate linear layers to apply the updates for the instance-level and pixel-level features (i.e.,  $\phi$  in Equation 1 from the main paper). We train and test with

8 updates, but we find that performance is similar if we train with 4 (and still test with 8).

**Visibility:** We use a linear layer to map the last update iteration’s pixel-level feature sequence into visibility logits.

**Optimization:** We train with a batch size of 4, distributed across four GPUs. At training time, we use a resolution of  $368 \times 496$ . For each element of the batch, we randomly sample 32 trajectories whose initial timestep is marked “visible” in the ground truth (so that the tracking targets always begin within-bounds and un-occluded). We train for 500,000 steps, with a learning rate of 1e-4 with a 1-cycle schedule [22], using the AdamW optimizer and clipping gradients to  $[-1, 1]$ . Training takes approximately 5 days on four GeForce RTX 2080s.

**Hyperparameters:** We use  $T = 8$  (timesteps considered by the MLP-Mixer), and  $K = 8$  (update iterations). The model can in general be trained for any  $T$ , but we found that the model was more difficult to train at  $T = 16$  and  $T = 32$ , likely because the complexity of trajectories grows rapidly with their length under our model, as there is no weight sharing across time. On the other hand, the temporal sensitivity allows our model to learn more complex temporal priors. We found that  $K > 8$  performs similar to  $K = 8$ , and so use  $K = 8$  because it is faster.

**Complexity:** *Speed:* When the number of targets is small enough to fit on a GPU (e.g., 128 targets for a 12G GPU), our model is faster than RAFT (340ms vs. 2000ms at  $480 \times 1024$ ). RAFT is comparatively slow because (1) it is too memory-heavy to compute all frames’ flows in parallel, so we must run it  $T - 1$  times, and (2) much computation is spent on non-target pixels. *Memory:* Our model’s memory scales with  $T \cdot N$ , where  $N$  is the number of particles being tracked, due to the iterated MLP-Mixer which consumes a  $T$ -length sequence of features per particle.

**Code:** DPV is implemented in Pytorch [17]. We will publicly release the code for the model and training procedure.

## 5. Experiments

We train our model in a modified version of FlyingThings [16], which we name FlyingThings++ (discussed more below).

We evaluate our model on tracking objects in FlyingThings++, tracking vehicles and pedestrians in KITTI [6], tracking heads in a crowd in CroHD [25], and finally, propagating keypoints in animal videos in BADJA [1]. We visualize trajectory estimates in DAVIS videos in Figure 1, to illustrate the method’s generality, and visualize the estimates against ground truth in Figures 4 and 3.

In the supplementary we include video visualizations of our results on these datasets, and also evaluate the effect of visibility-aware trajectory linking instead of naive linking.

## 5.1. Training data: FlyingThings++

We created a synthetic dataset based on FlyingThings [16], which is a dataset typically used to train optical flow models (usually in combination with other datasets). We chose FlyingThings because (1) its visuals and motions are extremely complex, which gives hope of generalizing to other data, and (2) it provides 10-frame videos with ground-truth forward and backward optical flow (as opposed to 2-frame videos), from which we can mine multi-step trajectory ground truth.

To create ground truth multi-frame trajectories, we chain the ground-truth flows forwards, and discard chains that fail a forward-backward consistency check (e.g., by landing on occluders). Through this process we create a sparse set of 4-frame and 8-frame trajectories. To this set we also add 2-frame trajectories from the raw flow fields.

The forward-backward consistency check ensures that the trajectories are accurate, but it leaves us with a library of trajectories where the target is visible on every timestep. Therefore, it is necessary to add *new occlusions* on top of the video. We do this on-the-fly during batching: for each FlyingThings video in the batch, we randomly sample an object from an alternate FlyingThings video, paste it directly on top of the current video, overwriting the pixels within its mask on each frame. We then update the ground-truth to reflect the new visibility in the occluded area on each frame, as well as update the trajectory list to include the trajectories of the added object.

Combining all videos with at least 32 valid 8-frame trajectories, we obtain a total of 4311 training videos, and 734 test videos. To expand the breadth of the training set, we augment the data on-the-fly with color and brightness changes, random scale changes, random crops which randomly shift across time, random Gaussian blur, and random horizontal and vertical flips.

## 5.2. Baselines

In our experiments we consider the following baselines.

**Recurrent All-Pairs Field Transforms (RAFT)** [26] represents the state-of-the-art in optical flow estimation, where a high resolution flow field is refined through iterative updates, based on lookups from a 4D cost volume constructed between all pairs of pixels. Note that similar to our method, RAFT has been trained on FlyingThings (including occlusions and out-of-bounds motions), but only has a 2-frame temporal span. To generate multi-frame trajectories with RAFT at test time, we compute flow with all consecutive pairs of frames, and then compute flow chains at the pixels queried on the first frame. To continue chains that travel out of bounds, we clamp the coordinates to the image bounds and sample at the edge of the flow map.

**DINO** [3] is a vision transformer (ViT-S [4] with patch size 8) trained on ImageNet with a self-supervision objec-

tive based on a knowledge distillation setup that builds invariance to image augmentations. To use this model for multi-frame correspondence, we use the original work’s code for instance tracking, which uses nearest neighbor between the initial frame and the current frame, as well as nearest-neighbor between consecutive frames, and a strategy to restrict matches to a local neighborhood around previous matches. We report results with and without this “windowing” strategy.

**TimeCycle** [32] learns correspondences between pixels from different frames by optimizing an objective that encourages correspondences to be cycle-consistent across time (i.e., forward-backward consistency), including across frame skips. This method tracks the same way as DINO, by computing feature affinity across frames and reporting nearest neighbors.

**Contrastive Random Walk (CRW)** [10] treats the video as a space-time graph, with edges containing transition probabilities of a random walk, and computes long-range correspondences by walking across the graph. Similar to TimeCycle [32], the model is trained with cycle-consistency.

**Memory-Augmented Self-supervised Tracker (MAST)** [14] learns correspondences between features by reconstructing the target frame with linear combinations of reference frames. At test time the correspondences are predicted autoregressively. The model is trained on OxUvA [29] and YouTube-VOS [35].

**Video Frame-level Similarity (VFS)** [34] learns an encoder that produces frame-level embeddings which are similar within a video, and dissimilar across videos. This model is trained on Kinetics-400 [13].

**ImageNet ResNet** [8] is a ResNet50 supervised for classification with ImageNet labels, and evaluated the same way as DINO.

## 5.3. Trajectory estimation in FlyingThings++

Using 8-frame videos from the FlyingThings++ test set as input, we estimate trajectories for all pixels for which we have ground-truth, and evaluate the Euclidean distance between each estimated trajectory and its corresponding ground truth, averaging over all 8 timesteps. We are especially interested in measuring how our model’s performance compares with the baselines when the target gets occluded or flies out of frame. To create controlled out-of-bounds and occlusion tests, we first take a central crop of each video, sized  $368 \times 496$ , providing us with some trajectories that fly out of the crop. Second, we implement a simple controllable occlusion strategy, where we replace a  $200 \times 200$  square in frames 2-5 with gray pixels.

We compare our model against DINO [3], representing the state-of-the-art for feature matching, and RAFT [26], representing the state-of-the-art for flow. Table 1 shows the

Method	Vis.	OOB	Occ
DINO [3]	32.4	75.4	68.13
RAFT [26]	9.05	19.41	36.30
DPV(ours)	<b>7.19</b>	<b>18.48</b>	<b>18.41</b>

Table 1. **Trajectory estimation error in FlyingThings++.** DPV is more robust to targets moving out-of-bounds or becoming occluded.

Method	Veh.	Ped.
DINO [3]	12.5	11.5
RAFT [26]	5.6	5.4
DPV(ours)	<b>5.0</b>	<b>5.3</b>

Table 2. **Trajectory estimation error in KITTI.** DPV performs slightly better than RAFT; DINO lags behind both.

results across the different evaluations on the test set. DINO struggles across all splits and performs worse on occluded pixels than on visible ones. RAFT obtains high accuracy for visible pixels, but its errors increase as the occlusions become more difficult. Our model performs similarly to RAFT on visible pixels, but it is somewhat robust to occlusions. Inspecting the results manually (visualized in supplemental), we see that RAFT’s trajectories become “stuck” in the region of the added occluder, which makes sense because flows there do not reflect the motion of the targets. Our model, in contrast, is able to locate the targets after they re-emerge from the occluder, and inpaint the missing portions of the trajectories.

#### 5.4. Trajectory estimation in KITTI

We additionally evaluate on an 8-frame point trajectory dataset that we created from the “tracking” subset of the KITTI [6] urban scenes benchmark. To create 8-frame trajectories, we sample a 3D box annotation that has at least 8 valid timesteps, select a LiDAR point within the box on the first timestep, transform it in 3D to its corresponding location on every other step, and project this location into pixel coordinates.

In Table 2 we see that RAFT and our method perform approximately on par with one another (with our method winning by less than one point), but DINO’s error is nearly twice this. We evaluate separately on vehicles and pedestrians since occlusions are more common with pedestrians, but we note that pedestrians also move more slowly, so the average errors are similar. Qualitative results for our model are shown in Figure 3-middle.

Method	Vis.	Occ.
DINO [3]	21.84	43.34
RAFT [26]	12.24	21.16
DPV(ours)	<b>8.26</b>	<b>15.93</b>

Table 3. **Trajectory estimation error in CroHD.** DPV achieves better accuracy, for both visible and occluded targets.

#### 5.5. Trajectory estimation in CroHD

We additionally evaluate on the Crowd of Heads Dataset (CroHD) [25], which consists of high-resolution (1920 x 1080) videos of crowds, with annotations tracking the heads of people in the crowd. We evaluate on 8-frame sequences extracted from the dataset, using an FPS of 12.5. We filter out targets whose motion is below a threshold distance, and split the evaluation between targets that are visible and those that undergo occlusions. The results are shown in Table 3. In this data, DPV outperforms RAFT and DINO by a wide margin, both visibility settings. DINO struggles overall, likely because the motions in this dataset are small, and DINO is only able to track at a coarse resolution. Qualitative results for our model are shown in Figure 3-right.

#### 5.6. Keypoint propagation in BADJA

BADJA [1] is a dataset of animal videos with keypoint annotations. These videos overlap with the DAVIS dataset [18], but include keypoint annotations. Keypoint annotations exist on approximately 1/5 frames, and the standard evaluation is Percentage of Correct Keypoint-Transfer (PCK-T), where keypoints are provided on a reference image, and the goal is to propagate these annotations to other frames. A keypoint transfer is considered correct if it is within a distance of  $0.2\sqrt{A}$  from the true pixel coordinate, where  $A$  is the area of the ground-truth segmentation mask on the frame.

We note that some existing methods test on a simplified version of this keypoint propagation task, where the ground-truth segmentation is available on every frame of the video (e.g., [37, 38]). Here, we focus on the harder setting, where the ground-truth mask is unknown. Similarly, we have found that feature-matching methods (e.g., [3]) constrain their correspondences to a local spatial window around the previous frame’s match. We report results for these methods with the qualifier “Windowed”, but focus again on the unconstrained version of the problem, where keypoints need to be propagated from frame 1 to every other frame, with no other knowledge about motion or position.

Table 4 shows the results of the BADJA evaluation. On four of the seven videos, our model produces the best keypoint tracking accuracy, as well as the best on average, by a margin of 9 points. DINO [3] obtains the best ac-



Figure 3. **Qualitative results in FlyingThings++ (left), KITTI (middle), and CroHD (right).** We visualize a video with the mean of its RGB. We trace the estimates with pink-to-yellow trajectories, and show ground truth in blue-to-green. FlyingThings++ is chaotic, but training on this data allows our model to generalize.

Method	bear	camel	cows	dog-a	dog	horse-h	horse-l	Avg.
Win. DINO [3]	<b>77.9</b>	69.8	<b>83.7</b>	<u>17.2</u>	46.0	29.1	50.8	<u>53.5</u>
Win. ImageNet ResNet [8]	70.7	65.3	71.7	6.9	27.6	20.5	49.7	44.6
Win. TimeCycle [32]	13.6	10.0	8.0	3.4	9.8	7.9	13.1	9.4
Win. CRW [10]	63.2	<u>75.9</u>	77.0	6.9	32.8	20.5	22.0	42.6
Win. VFS [34]	63.9	74.6	76.2	6.9	35.1	27.2	40.3	46.3
DINO [3]	<u>75.0</u>	59.2	70.6	10.3	<b>47.1</b>	35.1	<b>56.0</b>	50.5
ImageNet ResNet [8]	65.4	53.4	52.4	0.0	23.0	19.2	27.2	34.4
TimeCycle [32]	13.6	8.4	14.4	3.4	5.7	13.2	13.6	10.3
CRW [10]	66.1	67.2	64.7	6.9	33.9	25.8	27.2	41.7
VFS [34]	64.3	62.7	71.9	10.3	35.6	33.8	33.5	44.6
MAST [14]	51.8	52.0	57.5	3.4	5.7	7.3	34.0	30.2
RAFT [26]	64.6	65.6	69.5	13.8	39.1	<u>37.1</u>	29.3	45.6
DPV (ours)	72.7	<b>84.9</b>	<u>78.6</u>	<b>34.2</b>	<u>46.6</u>	<b>46.7</b>	<u>51.4</u>	<b>59.3</b>

Table 4. **PCK-T in BADJA.** In this evaluation, keypoints are initialized in the first frame of the video, and are propagated to the end of the video; PCK-T measures the accuracy of this propagation. In each column, we bold the best result, and underline the second-best. Above the middle bar, we give methods a spatial window (marked “Win.”) to constrain how they propagate labels, which encodes domain knowledge about the span of plausible motions in the domain (which is a common strategy in existing work). Below the bar, we run each method in the unconstrained setting. Our method wins in most videos, but DINO performs well also.

curacy in the remaining videos, though its widest margin over our model is just 5 points. Interestingly, windowing helps DINO (and other baselines) in some videos but not in others, perhaps because of the types of motions in DAVIS. We note that DAVIS has an object-centric bias (i.e., the target usually stays near the center of the frame), which

translation-sensitive methods like DINO can exploit, since their features encode image position embeddings; RAFT and DPV track more generally. In Figure 4 we visualize DINO, RAFT, and DPV trajectories on targets that undergo momentary occlusions, illustrating how DINO tracks only coarsely, and how RAFT loses track after the occlusion.

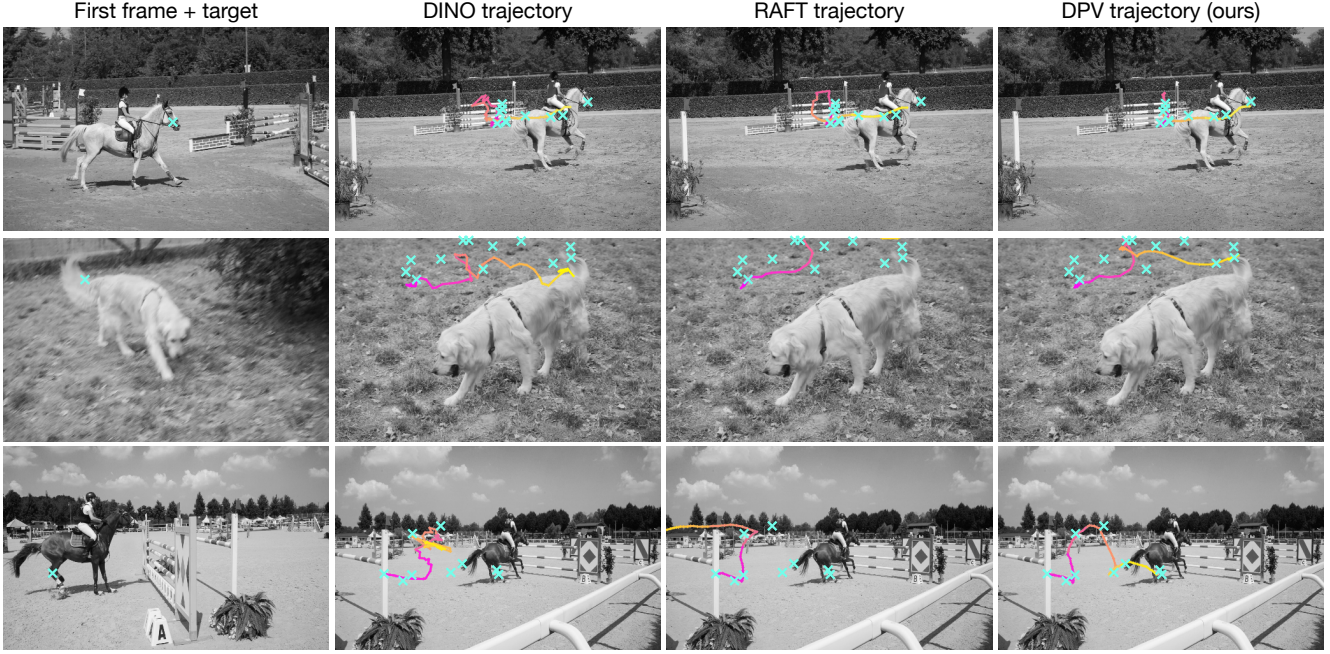


Figure 4. **Comparison with baselines in BADJA, on videos with occlusions.** For each method, we trace the estimated trajectory with a pink-to-yellow colormap. The sparse ground truth is visualized with cyan x’s. In the video on the first row, all methods perform fairly well, though DINO and RAFT drift slightly toward the horse’s body. In the second video, the target (on the dog’s tail) leaves the image bounds then returns into view. In the third video, the target (on the horse’s leg) is momentarily occluded, causing RAFT to lose track entirely. For a more detailed view of these results, please watch the supplementary video.

## 5.7. Limitations

Our model has two main limitations. First is our unique extreme tradeoff, of spatial awareness for temporal awareness. Although this maximizes the power of the temporal prior in the model, it sacrifices potentially valuable information that could be shared between trajectories. We are indeed surprised that single-particle tracking performs as well as it does, considering that spatial smoothness is known to be essential for accurate optical flow estimation. Extending our architecture to concurrent estimation of multiple point trajectories is a direct avenue for future work.

Our second main limitation stems from the MLP-Mixer. Due to this architecture choice, our model is not recurrent across time. Although longer trajectories can be produced by re-initializing our inference at the tail of an initial trajectory, our model will lose the target if it stays occluded beyond the model’s temporal window. We have tried models that are convolutional across time, and that use self-attention across the sequence length, but these did not perform as well as the MLP-Mixer on our FlyingThings++ tests. Taking advantage of longer and potentially varying temporal context would help the model track through longer periods of ambiguity, and potentially leverage longer-range temporal priors.

## 6. Conclusion

We propose Deep Particle Video (DPV), a method for multi-frame point trajectory estimation through occlusions. Our method combines cost volumes and iterative inference with a multi-frame temporal deep network, which jointly reasons about location and appearance of visual entities across multiple timesteps. We argue that optical flow, particle videos, and feature matches cover different areas in the spectrum of pixel-level correspondence tasks. Particle videos benefit from temporal context, which matching-based methods lack, and can also survive multi-frame occlusions, which is missing in flow-based methods. Given how tremendously useful optical flow and feature matching have been for driving progress in video understanding, we hope the proposed multi-frame trajectories will spark interest in architectures and datasets designed for longer-range fine-grained correspondences.

## 7. Acknowledgements

Toyota Research Institute, DARPA Machine Common Sense, and an NSF CAREER award provided funds to support this work.

## References

- [1] Benjamin Biggs, Thomas Roddick, Andrew Fitzgibbon, and Roberto Cipolla. Creatures great and SMAL: Recovering the shape and motion of animals from video. In *Asian Conference on Computer Vision*, pages 3–19. Springer, 2018. 5, 7
- [2] Thomas Brox and Jitendra Malik. Large displacement optical flow: Descriptor matching in variational motion estimation. *IEEE Transactions on Pattern Analysis and Machine Intelligence*, 33:500–513, 2011. 2
- [3] Mathilde Caron, Hugo Touvron, Ishan Misra, Hervé Jégou, Julien Mairal, Piotr Bojanowski, and Armand Joulin. Emerging properties in self-supervised vision transformers. In *ICCV*, 2021. 1, 6, 7, 8
- [4] Alexey Dosovitskiy, Lucas Beyer, Alexander Kolesnikov, Dirk Weissenborn, Xiaohua Zhai, Thomas Unterthiner, Mostafa Dehghani, Matthias Minderer, Georg Heigold, Sylvain Gelly, et al. An image is worth 16x16 words: Transformers for image recognition at scale. In *ICLR*, 2021. 4, 6
- [5] Alexey Dosovitskiy, Philipp Fischer, Eddy Ilg, Philip Hausser, Caner Hazirbas, Vladimir Golkov, Patrick Van Der Smagt, Daniel Cremers, and Thomas Brox. Flownet: Learning optical flow with convolutional networks. In *ICCV*, pages 2758–2766, 2015. 2
- [6] Andreas Geiger, Philip Lenz, Christoph Stiller, and Raquel Urtasun. Vision meets robotics: The kitti dataset. *International Journal of Robotics Research (IJRR)*, 2013. 5, 7, 12
- [7] Hugo Germain, Vincent Lepetit, and Guillaume Bourmaud. Visual correspondence hallucination: Towards geometric reasoning. In *arXiv Preprint*, 2021. 3
- [8] Kaiming He, Xiangyu Zhang, Shaoqing Ren, and Jian Sun. Deep residual learning for image recognition. In *Proceedings of the IEEE conference on computer vision and pattern recognition*, pages 770–778, 2016. 6, 8
- [9] Eddy Ilg, Nikolaus Mayer, Tonmoy Saikia, Margret Keuper, Alexey Dosovitskiy, and Thomas Brox. Flownet 2.0: Evolution of optical flow estimation with deep networks. *arXiv preprint arXiv:1612.01925*, 2016. 2
- [10] Allan Jabri, Andrew Owens, and Alexei A Efros. Space-time correspondence as a contrastive random walk. *Advances in Neural Information Processing Systems*, 2020. 2, 6, 8
- [11] Joel Janai, Fatma G’uney, Anurag Ranjan, Michael J. Black, and Andreas Geiger. Unsupervised learning of multi-frame optical flow with occlusions. In *European Conference on Computer Vision (ECCV)*, volume Lecture Notes in Computer Science, vol 11220, pages 713–731. Springer, Cham, Sept. 2018. 2
- [12] Wei Jiang, Eduard Trulls, Jan Hosang, Andrea Tagliasacchi, and Kwang Moo Yi. COTR: Correspondence Transformer for Matching Across Images. In *ICCV*, 2021. 3
- [13] Will Kay, Joao Carreira, Karen Simonyan, Brian Zhang, Chloe Hillier, Sudheendra Vijayanarasimhan, Fabio Viola, Tim Green, Trevor Back, Paul Natsev, et al. The kinetics human action video dataset. *arXiv:1705.06950*, 2017. 6
- [14] Zihang Lai, Erika Lu, and Weidi Xie. MAST: A memory-augmented self-supervised tracker. In *CVPR*, 2020. 1, 2, 6, 8
- [15] Z. Lai and W. Xie. Self-supervised learning for video correspondence flow. In *BMVC*, 2019. 2
- [16] N. Mayer, E. Ilg, P. Häusser, P. Fischer, D. Cremers, A. Dosovitskiy, and T. Brox. A large dataset to train convolutional networks for disparity, optical flow, and scene flow estimation. In *CVPR*, 2016. 2, 5, 6
- [17] Adam Paszke, Sam Gross, Francisco Massa, Adam Lerer, James Bradbury, Gregory Chanan, Trevor Killeen, Zeming Lin, Natalia Gimelshein, Luca Antiga, Alban Desmaison, Andreas Kopf, Edward Yang, Zachary DeVito, Martin Raison, Alykhan Tejani, Sasank Chilamkurthy, Benoit Steiner, Lu Fang, Junjie Bai, and Soumith Chintala. Pytorch: An imperative style, high-performance deep learning library. In H. Wallach, H. Larochelle, A. Beygelzimer, F. d’Alché-Buc, E. Fox, and R. Garnett, editors, *Advances in Neural Information Processing Systems 32*, pages 8024–8035. Curran Associates, Inc., 2019. 5
- [18] Jordi Pont-Tuset, Federico Perazzi, Sergi Caelles, Pablo Arbeláez, Alexander Sorkine-Hornung, and Luc Van Gool. The 2017 DAVIS challenge on video object segmentation. *arXiv:1704.00675*, 2017. 2, 7
- [19] Zhile Ren, Orazio Gallo, Deqing Sun, Ming-Hsuan Yang, Erik B Sudderth, and Jan Kautz. A fusion approach for multi-frame optical flow estimation. In *Proceedings of the IEEE Winter Conference on Applications of Computer Vision (WACV)*, 2019. 2
- [20] Agustín Salgado and Javier Sánchez. Temporal constraints in large optical flow estimation. In *International Conference on Computer Aided Systems Theory*, pages 709–716. Springer, 2007. 2
- [21] P. Sand and S. Teller. Particle video: Long-range motion estimation using point trajectories. In *CVPR*, volume 2, pages 2195–2202, 2006. 1, 3
- [22] Leslie N Smith and Nicholay Topin. Super-convergence: Very fast training of neural networks using large learning rates. In *Artificial Intelligence and Machine Learning for Multi-Domain Operations Applications*, volume 11006, page 1100612. International Society for Optics and Photonics, 2019. 5
- [23] Deqing Sun, Xiaodong Yang, Ming-Yu Liu, and Jan Kautz. PWC-Net: CNNs for optical flow using pyramid, warping, and cost volume. In *CVPR*, 2018. 2
- [24] Narayanan Sundaram, Thomas Brox, and Kurt Keutzer. Dense point trajectories by GPU-accelerated large displacement optical flow. In *ECCV*, 2010. 2
- [25] Ramana Sundararaman, Cedric De Almeida Braga, Eric Marchand, and Julien Pettre. Tracking pedestrian heads in dense crowd. In *CVPR*, pages 3865–3875, 2021. 5, 7, 12
- [26] Zachary Teed and Jia Deng. RAFT: Recurrent all-pairs field transforms for optical flow. In *European Conference on Computer Vision*, pages 402–419. Springer, 2020. 1, 2, 3, 4, 6, 7, 8
- [27] Zachary Teed and Jia Deng. RAFT: Recurrent all-pairs field transforms for optical flow. <https://github.com/princeton-vl/RAFT>, 2020. 5

[28] Ilya O. Tolstikhin, Neil Houlsby, Alexander Kolesnikov, Lucas Beyer, Xiaohua Zhai, Thomas Unterthiner, Jessica Yung, Daniel Keysers, Jakob Uszkoreit, Mario Lucic, and Alexey Dosovitskiy. MLP-mixer: An all-mlp architecture for vision. *ArXiv*, abs/2105.01601, 2021. 4

[29] Jack Valmadre, Luca Bertinetto, Joao F Henriques, Ran Tao, Andrea Vedaldi, Arnold WM Smeulders, Philip HS Torr, and Efstratios Gavves. Long-term tracking in the wild: A benchmark. In *ECCV*, pages 670–685, 2018. 6

[30] Ashish Vaswani, Noam Shazeer, Niki Parmar, Jakob Uszkoreit, Llion Jones, Aidan N Gomez, Łukasz Kaiser, and Illia Polosukhin. Attention is all you need. In *Advances in neural information processing systems*, pages 5998–6008, 2017. 4

[31] Qianqian Wang, Xiaowei Zhou, Bharath Hariharan, and Noah Snavely. Learning feature descriptors using camera pose supervision. In *Proc. European Conference on Computer Vision (ECCV)*, 2020. 3

[32] Xiaolong Wang, Allan Jabri, and Alexei A. Efros. Learning correspondence from the cycle-consistency of time. In *CVPR*, 2019. 1, 2, 6, 8

[33] Olivia Wiles, Sebastien Ehrhardt, and Andrew Zisserman. Co-attention for conditioned image matching. In *CVPR*, 2021. 3

[34] Jiarui Xu and Xiaolong Wang. Rethinking self-supervised correspondence learning: A video frame-level similarity perspective. In *Proceedings of the IEEE/CVF International Conference on Computer Vision (ICCV)*, pages 10075–10085, October 2021. 6, 8

[35] Ning Xu, Linjie Yang, Yuchen Fan, Jianchao Yang, Dingcheng Yue, Yuchen Liang, Brian Price, Scott Cohen, and Thomas Huang. Youtube-vos: Sequence-to-sequence video object segmentation. In *ECCV*, pages 585–601, 2018. 6

[36] Charig Yang, Hala Lamdouar, Erika Lu, Andrew Zisserman, and Weidi Xie. Self-supervised video object segmentation by motion grouping. In *ICCV*, 2021. 2

[37] Gengshan Yang, Deqing Sun, Varun Jampani, Daniel Vlasic, Forrester Cole, Huiwen Chang, Deva Ramanan, William T Freeman, and Ce Liu. LASR: Learning articulated shape reconstruction from a monocular video. In *Proceedings of the IEEE/CVF Conference on Computer Vision and Pattern Recognition*, pages 15980–15989, 2021. 7

[38] Gengshan Yang, Deqing Sun, Varun Jampani, Daniel Vlasic, Forrester Cole, Ce Liu, and Deva Ramanan. Viser: Video-specific surface embeddings for articulated 3d shape reconstruction. In *NeurIPS*, 2021. 7

## Supplementary Material

### A. Video attachment

The video attachment shows:

1. An overview of our method.
2. BAJDA keypoint propagation results, for DINO, RAFT, and DPV (our model), with trajectory trails for keypoints.
3. 8-frame trajectory estimates by DPV (our model) in DAVIS videos, with two types of visualization:
  - trajectory trails for pixels sampled at stride 8 over the first frame,
  - trajectory trails for pixels sampled at stride 4 within the ground-truth mask of an object on the first frame.

We make the following qualitative observations:

- DINO keypoints only coarsely track the target pixels, and appear to jitter unpredictably (e.g., see the legs of the horses), but typically stay within the correct region of the image frame.
- RAFT keypoints track the target pixels accurately, but consistently get caught on occlusions (e.g., see self-occlusion in the white dog causing all keypoints to end up on the dog’s edge).
- DPV keypoints track the target pixels with roughly the same accuracy as RAFT, but with better invariance to occlusions (e.g., see how the animal feet are sometimes tracked through leg-crosses, whereas crosses always cause failure for RAFT).

### B. Experiment details

In the trajectory estimation experiments, the trajectory estimation error is computed as the average of the L2 distance between point coordinates in the estimated trajectory and their corresponding ground truth.

**FlyingThings++:** Figure 5 shows visualizations of our results on the FlyingThings++ test data, compared to RAFT and ground truth. In this test data, the occluder is always in the middle of the image. We observe that RAFT trajectories get “stuck” in the middle of the frame, while our model is able to find the target after the occlusion and interpolate the trajectory.

**KITTI:** We preprocess the KITTI [6] data by resizing the original images (of slightly varying resolution) to  $512 \times 320$ . The data is at 10 FPS, and we use this framerate as-is. We use videos from sequences 0000-0009, which include mostly vehicles, as well as 0017 and 0019, which include mostly pedestrians. We filter the data to only include

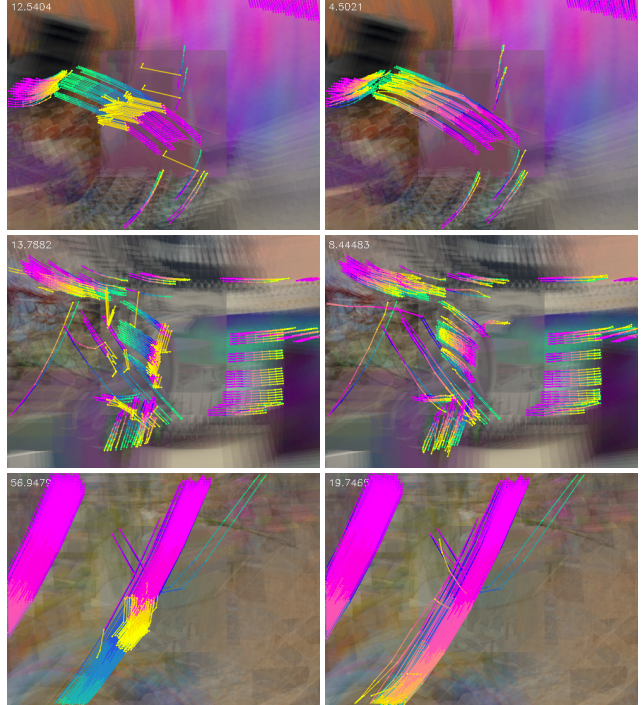


Figure 5. **Qualitative results in FlyingThings++** for RAFT (left column), and DPV (our model, right column). Trajectories are drawn in a pink-to-yellow colormap, over ground-truth trajectories which are in blue-to-green, and in the background is the mean RGB of the sequence. Note that RAFT trajectories get “stuck” in the middle of the frame, due to occlusions there. The value displayed in the top left corner is the average error in the video.

targets that undergo an occlusion by another object. We do this by checking if (1) the target’s box has an IOU greater than 0.5 with another annotated box, and (2) the target’s box is behind (i.e., has a larger depth-axis value than) the intersecting box. Note that since the annotations are only at the box level, this data does not evaluate fine-grained motions within the objects, such as the movement of the legs or arms of a pedestrian.

**CroHD:** We preprocess the CroHD [25] data by cropping the original images of size  $1920 \times 1080$  into crops of size  $512 \times 320$ . To make the data harder, we subsample the frames in the original dataset so that the FPS is reduced by a factor of 3. Since the dataset provides the ground truth for the head bounding boxes throughout the video and their visibility information, we define the ground truth point trajectory for a head as the trajectory of the center of its bounding box. In addition, we only test on heads that move (excluding ones that move less than 150px over the 8 frames). We test on sequences of 8 frames.

**Runtime:** On an 8-frame video with resolution  $480 \times 1024$ , the CNNs take approximately 6 ms, and the iterative inference for a batch of trajectories takes approximately 330

ms. If we require more trajectories than fit on the GPU simultaneously (e.g., if the GPU has 12G memory and we require more than 128 trajectories), we simply split the set into multiple batches, and compute one batch at a time. Note it is possible to share the CNN features across these batches. Also note that when a small number of trajectories is required, our model runs much faster than RAFT, since RAFT always computes results densely (at approximately 2000 ms per 8-frame video). That is, as long as the number of trajectories is small enough to fit on the GPU in parallel, then our total time is less than 340 ms; but time will extend linearly as we exceed GPU capacity and demand more computation in serial.

### C. Ablation on visibility-aware linking

In this section we evaluate the effect of visibility-aware trajectory linking instead of naive linking.

Our trajectory linking strategy relies on visibility estimates produced by the model. Without using these estimates, we may still link trajectories naively (i.e., greedily), by chaining the 8-frame trajectories end-to-end. We evaluate this choice in BADJA keypoint propagation, and show the result in Table 5. Naive linking indeed gives worse PCK-T, but the margin is only 0.2 points. This may suggest that the visibility estimator is not generalizing well to the new video domain. Alternatively, this may be showing a small effect because the metric is dominated by trajectories that stay visible for the full duration of the video, as evidenced by DINO obtaining 50.5 PCK-T with no strategy for managing occlusions at all (see Table 4 from main paper).

Method	Average PCK-T
Without visibility-aware linking	59.1
With visibility-aware linking	<b>59.3</b>

Table 5. **Effect of visibility-aware linking on keypoint propagation in BADJA.** Linking trajectories from locations estimated to be “visible” yields a small improvement in average PCK-T.

### D. Pseudocode

Algorithm 1 steps through the inference process of our method. This aims to add more detail to the process illustrated in Figure 2 of the main paper, including for example the multi-scale set of local correlation maps. We plan to publicly release our Pytorch code and pre-trained model weights.

---

#### Algorithm 1 Deep Particle Video pseudocode, Pytorch-like

```

# cnn = resnet cnn backbone
# mixer = mlp mixer
# linear = linear layer
def forward(rgbs, x1, iters=10):
    T, Ci, H, W = rgbs.shape # Ci==3
    D, = x1.shape # D==2

    # compute features for all frames
    feat_maps = cnn(rgbs) # (T,C,H/8,W/8)

    # get appearance of target
    f1 = sample(feat_maps[0], x1) # (C)

    # tile out first position & appearance,
    # to initialize the trajectory
    xs = x1.reshape(1,2).repeat(T,1) # (T,2)
    fs = fs.reshape(1,C).repeat(T,1) # (T,C)

    for itr in range(iters):
        # collect multi-scale local corrs
        # L = num_scales, P = patch_size
        corrs = pyramid_corr(feat_maps,
                              fs, xs,
                              L, P)
        corrs = corrs.reshape(T,-1) # (T,L*P*P)

        # concat everything; feed to mlp mixer
        tokens = cat([xs - xs[0:1],
                      feat_vecs,
                      corrs],
                     dim=1) # (T,2+C+L*P*P)
        deltas = mixer(tokens) # (T,2+C)

        # apply residual updates
        xs = xs + deltas[:, :, 2] # (T,2)
        fs = fs + deltas[:, :, 2] # (T,C)
        vis = sigmoid(linear(fs)) # (T,1)
        return xs, vis

```

---